Composite Structures 319 (2023) 117166

Contents lists available at ScienceDirect

Composite Structures

journal homepage: www.elsevier.com/locate/compstruct

Effects of post-fracture repeated impacts and short-term temperature gradients on monolithic glass elements bonded by safety films

Chiara Bedon [a,*], Filipe A. Santos [b]

[a] University of Trieste, Department of Engineering and Architecture, Trieste, Italy
[b] CERIS-NOVA, Department of Civil Engineering, NOVA School of Science and Technology, Universidade NOVA de Lisboa, Caparica, Portugal

ARTICLE INFO

Keywords:
Monolithic glass
Glass retrofit
Safety films
Post-fracture capacity
Cracked vibration frequency
Experiments
Dynamic identification
Analytical modelling
Finite Element (FE) numerical modelling

ABSTRACT

Weathering and operational conditions, as known, have significant impact on typical constituent materials which are used for many construction applications. Among others, structural glass solutions can suffer for these effects in terms of major modification of material properties of interlayers, bonds, connections, gaskets and polymeric components in general. In this paper, the attention is given to the effects of repeated low-amplitude impacts and short-term temperature gradients for the characterization of load-bearing capacity in monolithic glass elements retrofitted by safety films. Especially for existing glass systems which are made of monolithic glass with limited strength and resistance capacity against ordinary and accidental mechanical loads, safety films are commercially available for retrofit interventions. They are primarily expected to keep together glass fragments in case of breakage, and thus minimize possible injuries. Besides, after first fracture, the so obtained glass-film composite elements have uncertain residual mechanical capacity against ordinary loads, given that it mostly depends on thin films composed of Polyethylene terephthalate (PET)-layers and pressure sensitive adhesives (PSAs). To this aim, a set of experiments (for a total of 950 configurations) is carried out in laboratory conditions (30 °C) on small-scale samples of fractured annealed monolithic glass elements bonded by commercial safety films, under repeated low-amplitude impacts / vibrations (S1-TR series), or additionally subjected to preliminary short-term thermal gradients (S2-TC1 series cooled at +5 °C and S3-TC2 series at −20 °C). Localized impacts are quantified in acceleration peaks in the range of 2 ÷ 14 m/s^2 and rotations at supports in the order of 15 ÷ 20°. The interpretation of dynamic experimental results is carried out in terms of post-fracture vibration frequency (based on classical operational modal analysis techniques) and used, with the support of simplified analytical models or Finite Element (FE) numerical simulations, to characterize the response of cracked glass-film samples. Most importantly, the vibration frequency decrease is used to quantify their residual load-bearing capacity under unfavourable conditions, and to quantify the post-critical benefit of thin bonding safety films under unfavourable conditions.

1. Introduction

Connections in structural glass applications can take the form of several technological solutions, which include in most of case the use of adhesives, bonds and viscoelastic materials [1]. Regardless their composition and detailing, connections and many components of glass solutions for buildings are sensitive to weathering conditions and operational conditions, as well as ageing. This problem is relevant for glass but for engineering applications in general. To this aim, an increasing number of research studies has been dedicated to the experimental, analytical and Finite Element (FE) numerical analyses for specific construction components and configurations [2]. For specific applications in the field of structural glass, literature studies and examples include durability aspects [3], ageing phenomena [4], capacity assessment of embedded connections [5–7] and a multitude of many other investigations to support the optimal design of new glass solutions.

Under the above considerations, a major uncertainty is still represented by existing / in-service glass systems, which have been assembled before the definition and availability of specific standards for structural design or retrofit technologies, and thus can offer only limited capacity to typical mechanical design actions. Especially for monolithic glass, the use of safety films to prevent critical shards in case of fracture is a

* Corresponding author.
E-mail address: chiara.bedon@dia.units.it (C. Bedon).

https://doi.org/10.1016/j.compstruct.2023.117166
Received 15 January 2023; Received in revised form 14 April 2023; Accepted 16 May 2023
Available online 20 May 2023

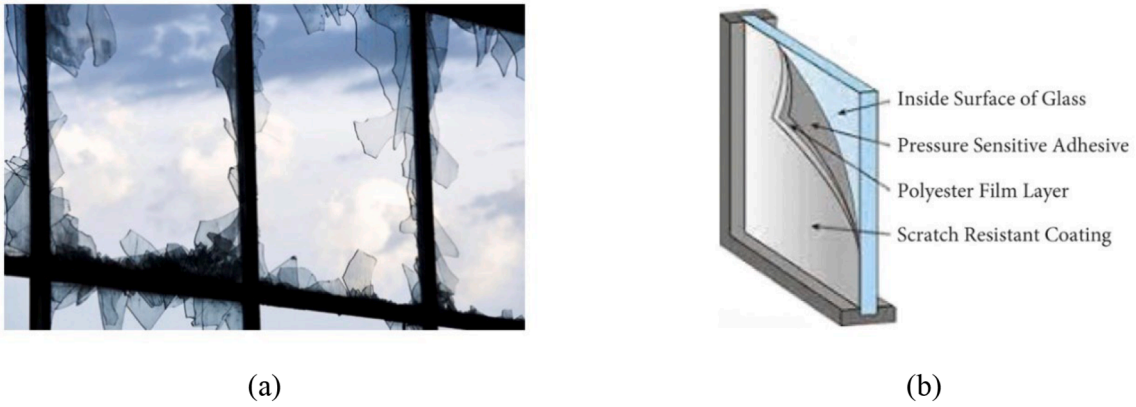

Fig. 1. Glass window under hazard: (a) fracture pattern and (b) schematic drawing of safety film (figure reproduced from [9] under the terms and conditions of CC-BY license agreement).

relatively recent and still not fully addressed research topic. These films are mostly based on Polyethylene terephthalate (PET)-layers and pressure sensitive adhesives (PSAs). Given that these films are used to minimize possible risk for customers and reduce the hazard in post-fracture stage due to cracked glass elements, a major attention is required for the evaluation of their actual characteristics and potentials [8,9]. Also, attention should be paid against aging effects on their capacity [10]. Chemical and mechanical characterization based on different techniques, such as Differential Scanning Calorimetry (DSC), Fourier Transform Infrared spectroscopy (FT-IR), tensile tests and peeling tests, was thus reported in [8–10] for small-scale samples under artificial aging in terms of high humidity or high temperature (including water immersion in vacuum box or heating exposure at 50 °C, 70 °C or 100 °C). The post-fracture out-of-plane bending response of glass-film samples was also preliminary addressed in [10], in terms of load-bearing capacity under artificial aging.

As a further extension of earlier studies, the present investigation aims at exploring the residual capacity in post-critical stage for film-retrofitted monolithic glass elements, and thus to support possible optimization of retrofit interventions, as well as to support a quantitative assessment of residual capacities and vulnerability.

Ambient conditions and temperature gradients are known to represent major influencing parameters for structural glass applications, especially when they are combined to polymers. To this aim, several literature efforts have been elaborated in last years to characterize the mechanical features and residual load-bearing capacity of various structural glass components and solutions under imposed artificial or natural aging protocols. On the other side, most of existing studies are typically related to laminated glass elements or special connections for glass applications, and minimum attention is given to the mechanical assessment of retrofit strategies or to the vulnerability analysis of in-service glass systems. Volakos et al. [11] tested novel embedded liquid-laminated connections for glass, at −10 °C or +50 °C under pull-out test setup, giving evidence of typical mechanical features and failure mechanisms. The effect of temperature on typical interlayers for glass laminates have been largely investigated, see for example [12–15], with major attention for temperatures up to 60–80 °C under long-term exposure time intervals. Special films and coatings for glass applications have been rather scarcely investigated in the literature, and for example few selected solutions have been chemically characterized in [16,17]. Benefits of safety films for glass elements under impact have been experimentally and numerically investigated in [18,19]. The present study, in this regard, applies the safety films characterized in [8–10] in a post-fracture scenario to quantify the expected load-bearing performance of retrofitted glass elements, by accounting for possible influence due to imposed thermal gradients.

In parallel to aging and unfavourable ambient conditions, most importantly, this paper explores the effect of imposed repeated impacts for the assembled glass-film samples, so as to quantify the residual capacity after first breakage, and thus the expected safety levels after critical accidents. Repeated impacts and vibrations are in fact known to strongly affect the durability and efficiency of retrofit interventions, and this has been addressed for various engineering applications and structural details [20–22], but not for film-retrofitted glass elements. According to literature [23–26], both unfavourable ambient conditions and repeated impacts in laminated glass assemblies are typically responsible of progressive bonding deterioration, and thus manifest in possible delamination of constituent layers, with major consequences on the actual bending stiffness of the composite section and on the expected load-bearing capacities. This condition represents a major risk for functionality and safety preservation, and should be possibly monitored and quantified. Among others, it was proved in [23–26] that the fundamental vibration frequency (and its modification) can be used to efficiently measure – based on dynamic inverse detection techniques – possible delamination phenomena (and even damage) in composite glass systems [27,28].

To this aim, the present investigation focuses on small-scale samples which are assembled with the same components characterized in [8,9], that is consisting of monolithic glass panes bonded by a commercial safety film explored in [8–10]. However, differing from previous efforts, the primary goal of current investigation is represented by the experimental analysis and characterization of glass-film composite samples under repeated low-amplitude impacts / vibrations (after first breakage) and various short-term temperature gradients. Such a test setup (small-scale detail) is chosen to be representative of a real post-critical application in buildings, where the cracked glass fragments are kept in position by safety films (Fig. 1) and the composite glass-film system should be able to offer a minimum residual capacity before maintenance interventions.

Non-destructive dynamic experiments are carried out on a set of preliminary fractured, small-scale samples under a simply support configuration. Realistic post-critical configurations of glass-film composite elements are reproduced by hammer, to account for possible interlock of fragments, as it could happen in constructed facilities after damage (i.e., Fig. 1).

Glass-film samples are thus subjected to repeated, low-amplitude, localized impacts and explored based on classical dynamic identification techniques (Section 2). A primary attention in the analysis of experimental results is given to the prediction of post-fracture fundamental vibration frequency $f_{1,cr}$ and its sensitivity to repeated impacts / temperature gradients (Section 3). Additional support for the interpretation of test evidences is also derived from dedicated FE numerical analyses (Section 4), including parametric studies in terms of vibration frequency sensitivity and heat transfer simulations, to quantify the

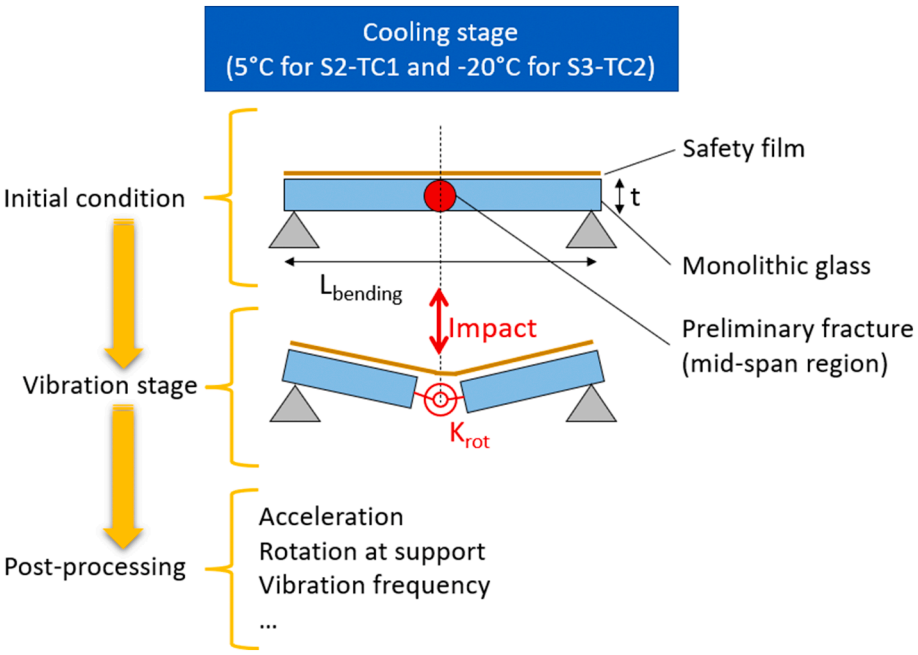

Fig. 2. Schematic setup for the present experimental investigation ($L_{bending}$ = 95 mm, t = 6 mm).

temperature distribution in the tested samples, and its correlation with load-bearing performances.

2. Experimental methods

For the present investigation, a primary role was assigned to vibration experiments. The measurement of acceleration records for specimens under vibrations was properly combined with dynamic identification techniques, so as to characterize the mechanical properties of bonding films under dynamic loads. For the selected setup configurations and specimens, more in detail, the investigation was qualitatively carried out as in Fig. 2.

The schematic drawing gives evidence of the initial condition of intact (pre-cracked) glass-film composite samples, as well as the expected behaviour under imposed vibrations, in the post-cracked stage. Once glass samples were deliberately fractured around mid-pan in the preliminary preparation stage, the vibration analysis was carried out on composite samples in which two major glass parts were considered bonded by the safety film only, which was used to provide the structural continuity and mechanical interaction of glass fragments.

Glass portions, more precisely, were assembled to freely bend under tensile (sagging) bending loads as in Fig. 2, while possible mechanical interaction (if any) could occur under compressive (hogging) bending moments only (due to contact of fragments in compression). When the specimen bends like in the schematic setup of Fig. 2, the fractured shards are in fact fully separated in tension, while any kind of interposed gap can be closed under compression. Due to the presence of bonding film, moreover, the tensile side mechanism is the most influencing for the vibration performance of the glass sample, and it is thus mostly responsible of the final fundamental frequency and dynamic mechanical parameters of the composite system.

In this regard, a simple modelling strategy aimed at exploring the interfacial stresses and force components could be possibly developed by introducing an equivalent spring with rotational stiffness K_{rot} and able to reproduce the physical contact phenomena of glass fragments only, that is null stiffness in tension ($K_{rot} = 0$) and rigid contact mechanism (if any, otherwise $K_{rot} = 0$ as in present study) in compression [9]. Under similar assumptions, the bending stiffness of the composite glass-film section is fully governed by partial bonding offered by safety film to glass fragments, and can be extrapolated by investigating the dynamic response of the system [9].

For present study, a primary attention was given to dynamic identification for the system components as in Fig. 2, based on classical operational modal analysis methods [28]. The basic assumption is that

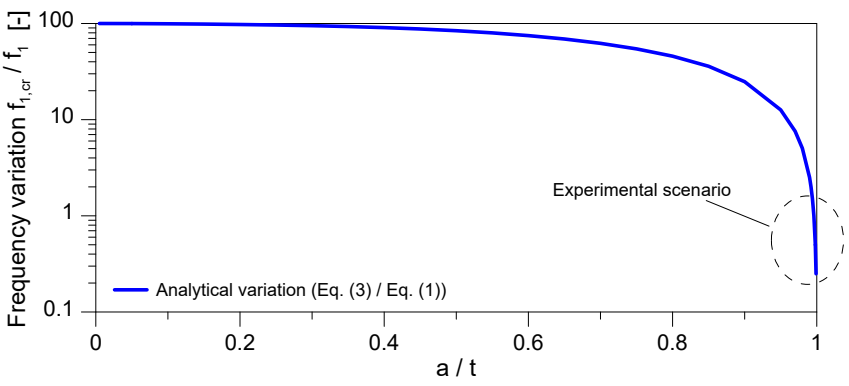

Fig. 3. Analytical trend of post-fracture fundamental frequency variation for the presently examined glass-film samples, based on Eqs. (1) and (3).

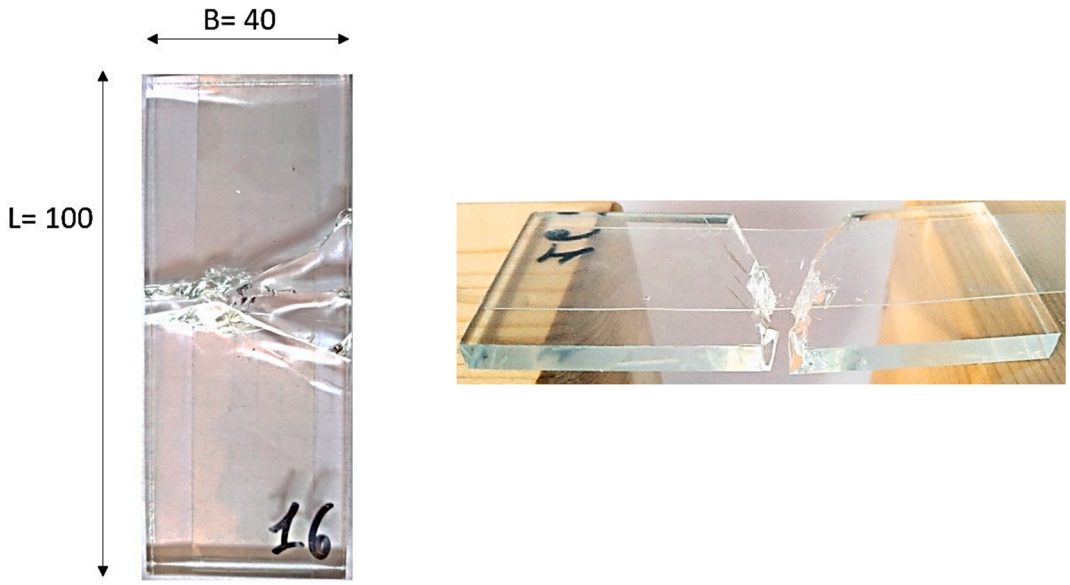

Fig. 4. Example of glass-film sample: (a) initial configuration and (b) cracked scenario after repeated dynamic tests. Dimensions in mm.

for a simply supported composite glass-film system the fundamental (uncracked) vibration frequency is proportional to its equivalent bending stiffness, given that for a monolithic t section it is [23,28,29]:

$$f_1 = \frac{\omega_1}{2\pi} = \frac{\pi}{2L_{bending}^2}\sqrt{\frac{EJ}{\rho A}} \tag{1}$$

with ω_1 the angular frequency, E the modulus of elasticity (MOE), J the second moment of area, A the cross-section, ρ the material density. The analytical result from Eq. (1) represents an ideal upper limit for glass components which may be affected by possible delamination, support flexibility or degradation, damage, etc. [23,28,30]. In case of a single major crack as in the present investigation (Fig. 2), the corresponding cracked frequency can be estimated in accordance with [31], that is:

$$f_{1,cr} = f(f_1,\ crack\ size,\ crack\ depth,\ crack\ position,\ etc.) \tag{2}$$

Assuming that the crack is located at mid-span section and has propagation $a = 0 \div t$ through the thickness t of glass, Eq. (2) takes the form [31]:

$$f_{1,cr} = f_1\sqrt{\frac{1+2\eta}{1+4\eta+(\pi^4/24)\eta}} \tag{3}$$

with:

$$\eta = \frac{t}{L_{bending}}m(a/t) \tag{4}$$

where the function $m(a/t)$ is given by:

$$m\left(\frac{a}{t}\right) = 2\left(\frac{a/t}{1-a/t}\right)^2\left[5.93 - 19.69\left(\frac{a}{t}\right) + 37.14\left(\frac{a}{t}\right)^2 - 35.84\left(\frac{a}{t}\right)^3 + 13.12\left(\frac{a}{t}\right)^4\right] \tag{5}$$

For the presently examined samples, the variation of post-fracture frequency (i.e., Eq. (3) / Eq. (1)) follows the trend in Fig. 3. To note that when $a/t = 0.999$, the post-fracture frequency is estimated in $f_{1,cr} = 3.59$ Hz from Eq. (3), which correspond to $f_{1,cr} / f_1 = 0.24$ (with $f_1 = 1440$ Hz for the uncracked samples, that is $a/t \rightarrow 0$).

3. Experimental analysis

3.1. Specimens

The experimental analysis was carried out at the University of Trieste, Department of Engineering and Architecture (Italy). Following Fig. 2, the typical specimen consisted of a monolithic, annealed glass element with $L = 100$ mm $\times$ $B = 40$ mm $\times$ $t = 6$ mm dimensions. The use of monolithic glass was privileged to laminated sections, in order to facilitate the computational process and exclude additional possible uncertainties (i.e., viscoelastic phenomena in the interlayers, debonding, etc. [12,23,26,32–35]). All the specimens were characterized by the presence of a thin layer of safety film on the top [8,9], like in Fig. 2. A commercial multi-layer film for safety glass applications was used [8–10], which is characterized by 0.35 mm total thickness. Also, it is composed by two different layers made of PET, with a thickness of 0.11 mm and 0.22 mm respectively, and a PSA adhesive that was protected by environmental conditions by means of a removable release liner [8,9].

Before the execution of dynamic experiments, a preliminary crack like in Fig. 2 was also imposed to glass elements, by hammer. In this regard, it is important to highlight that the use of float annealed glass was chosen to allow the propagation of few major cracks in the original samples. Moreover, glass-film samples were deliberately fractured by hammer in order to reproduce, even at a small-scale level, a realistic post-fracture configuration, that is inclusive of possible interlocking phenomena for fragments. Fig. 4 shows typical examples of glass-film configurations in the initial stage of vibration testing (with all fragments still kept in position by the safety film) and after repeated dynamic tests.

3.2. Preparation of glass-film specimens

The monolithic glass specimens were bonded to safety films with 35 mm in width and 120 mm in length. The width of bonding strips was kept identical to experimental samples characterized in [8–10]. The preparation was based on dry lamination procedure, and carried out in uncontrolled room conditions, before the execution of experiments. A strip was applied on the rigid glass substrate with high pressure, in order to make perfectly adherent the two materials. The adhesion stage was realized with careful attention to avoid the creation of bubbles and

Table 1
Summary of experimental configurations for cracked glass-film composite samples.

			Series		
			S1-TR	S2-TC1	S3-TC2
Preliminary cooling stage	Time interval	[h]	–	3	3
	Temperature	[°C]	–	5	−20
Dynamic tests	N. of impact configurations	–	335	590	25
	N. of samples	–	7	7	2
	N. of cycles	–	7	7	7

superficial folding. To minimize the influence of possible impurities or inclusions, the glass surface was treated and the protection film was quickly peeled off. Then, pressure was manually applied to the film to remove any residual heterogeneity and make the adhesion as much homogeneous as possible.

As a key step of the investigation, the glass specimens bonded with safety film were deliberately fractured before the execution of dynamic experiments. A steel hammer was used to fracture the glass plates in the mid-span region (single major crack, with $a/t \approx 1$). To this aim, each sample was temporarily bedded on a rigid substrate, and a single hammer hit was imposed to glass. The advantage associated to the presence of the bonding film, at the time of fracture, was to keep together the glass fragments for the subsequent dynamic tests. In addition, the use of hammer for fracture was preferred to glass cutting in order to account for a more realistic post-fracture impact configuration (with possible minor fragments, interlocking, etc.).

To note that individual samples were tested under more than a single impact, in order to extend the dataset of scenarios and to quantify the residual capacity modification as a function of repeated vibrations. A typical fractured scenario representative of the initial configuration for the dynamic experiments can be seen in Fig. 4, where the structural continuity of shards is ensured by the safety film only, depending on its adhesive properties.

3.3. Experimental protocol and configurations

All the experiments were carried out in a laboratory setup. The room temperature at the time of experiments was measured in 30 °C (Summer), and the available samples were grouped by three series. For S1-TR series, the dynamic experiments were carried out at room temperature (30 °C, at the time of experiments), without any preliminary thermal treatment. For S2-TC1 and S3-TC2 series, in contrary, dynamic tests were still carried out in room conditions (30 °C), but after a preliminary cooling stage. This phase included an imposed time interval for cooling the samples (at 5 °C for 3 h for S2-TC1 specimens, or at −20 °C for 3 h for S3-TC2 specimens respectively).

Vibration experiments were carried out by positioning the specimens on lateral supports like in Fig. 2, and testing them under localized impacts. Impacts were repeatedly imposed in the mid-span region of samples (see also Section 3.4), based on random finger hits able to produce low-amplitude vibrations and allow the inverse derivation of dynamic parameters for the examined systems [23,30].

For S1-TR samples, the experimental outputs were measured at room temperature under different acceleration ranges / vibration amplitudes, for a total of 335 configurations (Table 1). For S2-TC1 and S3-TC2 samples, an identical experimental approach was taken into account, with the only difference represented by the preliminary cooling stage. These samples were in fact tested in dynamic setup after a given time interval Δt from preliminary cooling, to allow for a certain temperature increase ΔT, from the cooling setup to room condition. In this case, the temperature at the time of vibrations was also recorded.

In total, 950 impact configurations were investigated for the three series of samples. A summary of testing configurations is proposed in Table 1. A number of 16 similar specimens was taken into account, thus each sample was subjected to repeated low-amplitude impact cycles and repeated vibrations.

3.4. Instruments

The experimental study was based on classical dynamic identification techniques as in [28], by taking into account previous engineering knowledge and experimental characterization of safety films reported in [8–10].

For the setup schematized in Fig. 5, a small MEMS sensor was rigidly fixed at the support of each specimen, to avoid any interference with the mid-span mechanism of fragments in bending.

Three-component acceleration histories were measured with a sampling rate of 200 Hz. Meanwhile, the rotation angle (in degrees) about a local reference system as in Fig. 5 (b) was also measured during the experiments. The limited size and weight of the sensor in use ensured the negligible influencing effect of the instrument on the vibration response of the specimens. The mini device in use, more in detail, consisted of a commercial sensor based on IMU AHRS MPU6050 chip board, wireless, three-axes accelerometer sensor and inclinometer (±16 g its range, 0.005 g the resolution, 0.2 ÷ 200 Hz the available sampling rate). The sensor is equipped by integrated battery and embedded microcontroller, ARM® Cortex®-M0 single core type (32 bit, clock frequency up to 48 MHz). The size of MEMS sensor was measured in 36 × 36 mm, with 15 mm its thickness and 20 g the weight. The imposed impacts were quantified on glass-film samples acceleration peaks in the range of 2 ÷ 14 m/s^2, and a maximum rotation angle of 15 ÷ 20°.

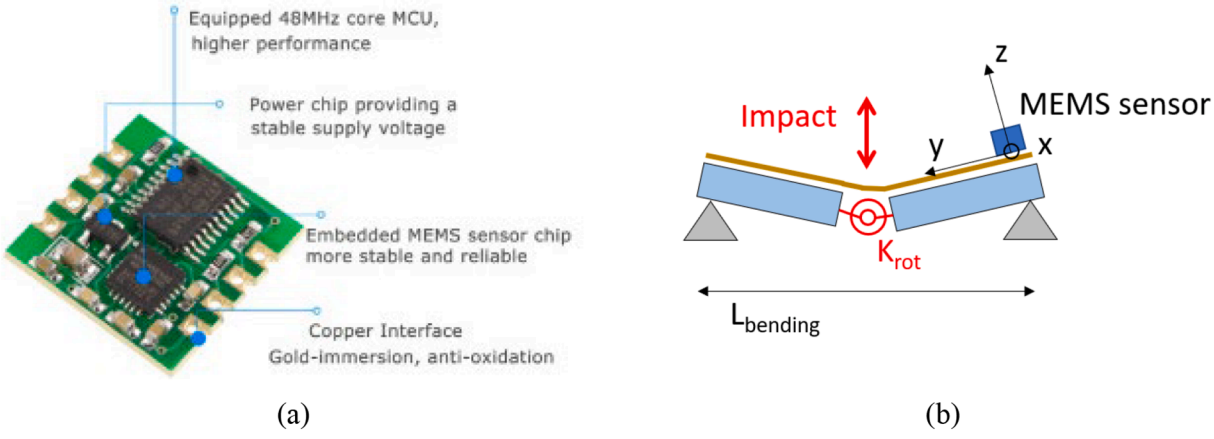

Fig. 5. Experimental methods: (a) detail of tri-axial MEMS sensor (figure adapted from [30]) and (b) typical setup ($L_{bending}$ = 95 mm).

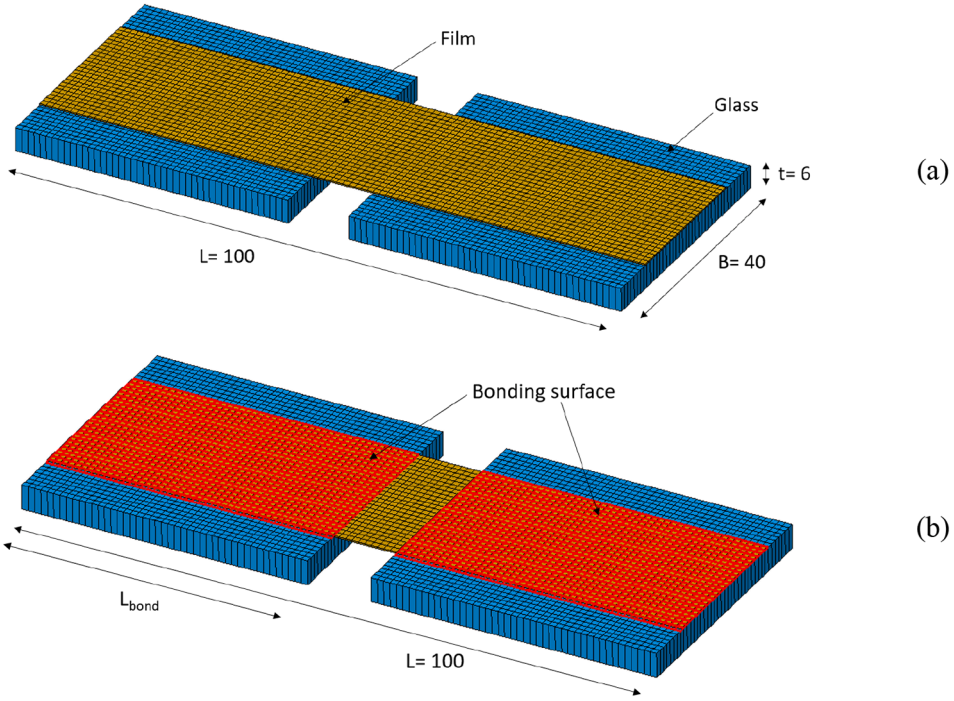

Fig. 6. Simplified numerical model (extruded view): (a) geometry and layout, with (b) bonding surfaces (ABAQUS). Dimensions in mm.

3.5. *Numerical assessment of experiments*

In support of experimental analysis and interpretation of results, a first, simplified FE model was developed in ABAQUS/Standard [36], in order to reproduce the reference glass-film sample configuration and predict the expected vibration frequency under imposed impact conditions. According to [9], the major simplification was carried out in terms of geometrical description of glass fragments, compared to experimental geometries like in Fig. 4. The reference model included in fact two glass portions representative of actual fragments (based on local / average measurement of samples), thus corresponding to $a/t = 1$ major crack in Eq. (3), and the nominal size of bonding film (Fig. 6).

Based on early sensitivity analysis of mesh size, a regular pattern was used both for glass and film parts, with reference seed in the range of 0.35 mm and up to 1 mm. This choice resulted in 6,500 elements for the assembly in Fig. 6, with 38,500 degrees of freedom. Shell elements (S4R type) and brick elements (C3D8R type), respectively, were used for glass and films.

For the purpose of vibration frequency estimates, input material properties were described based on linear elastic constitutive models. The use of equivalent linear elastic material properties for both components, and especially for the bonding film, was justified by earlier experimental characterization under various ageing and strain rate conditions, including tensile tests, peeling tests and bending tests [8–10]. Whilst representing a simplified mechanical characterization, such an approach is in line equivalent stiffness assumptions of typical use for the analysis of laminated glass elements under well-defined operational conditions [37], and can preliminarily avoid – especially for inverse detection studies – the use of complex constitutive models [27,38].

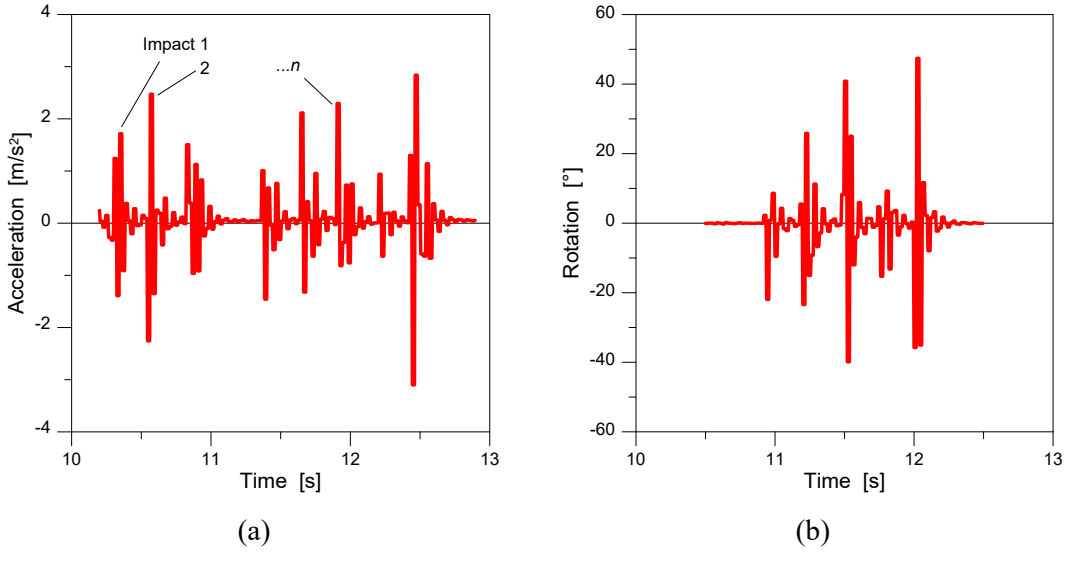

Fig. 7. Example of experimental measurements: (a) vertical acceleration record and (b) rotation at the support history.

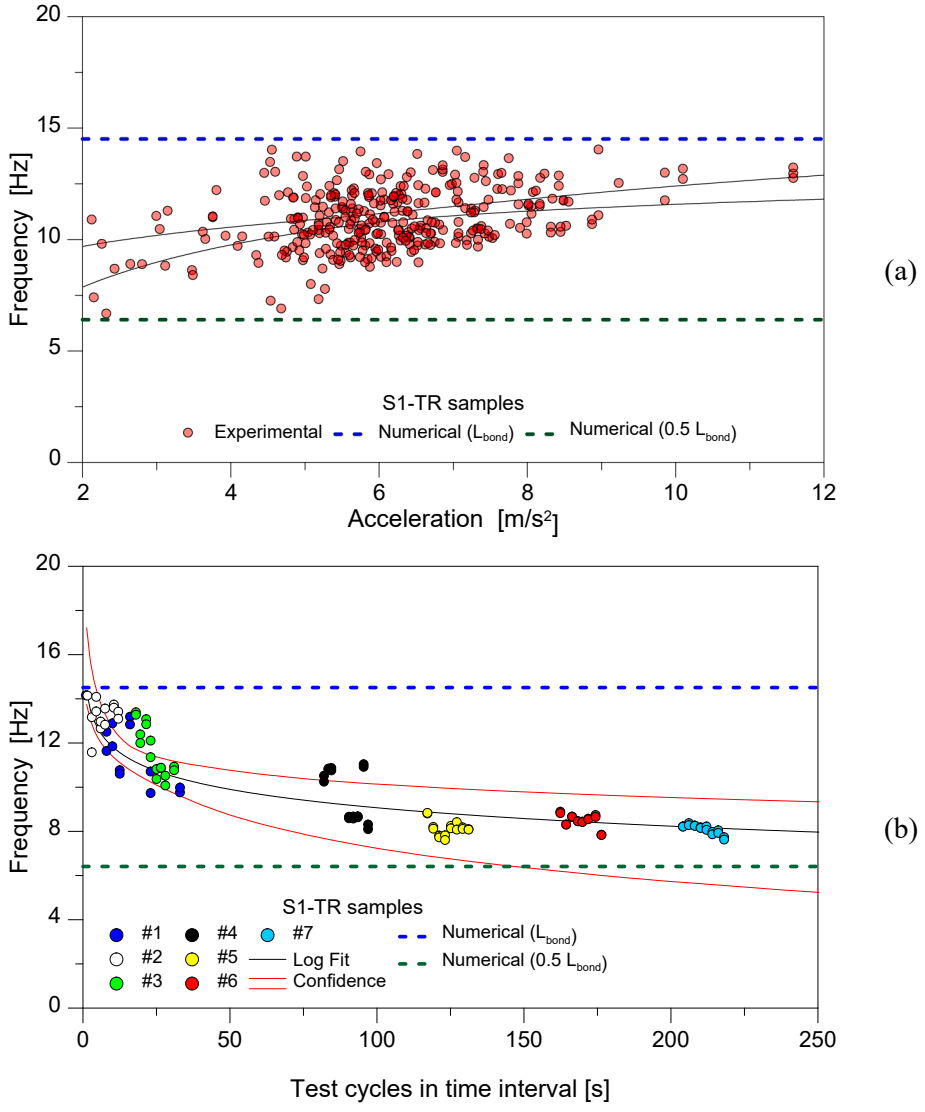

Fig. 8. Experimental results for S1-TR samples (room temperature) and comparison with FE numerical estimates (ABAQUS): (a) frequency-acceleration and (b) frequency-repetition trends.

In case of annealed glass, the modulus of elasticity was set in 70 GPa, with 0.23 the Poisson' ratio and 2500 kg/m^3 the density [39]. The safety film was mechanically described based on the experimental outcomes reported in [9], that is ≈ 3 GPa for the modulus of elasticity, 0.35 the Poisson' ratio and 1350 kg/m^3 the density. In the preliminary stage, moreover, a rigid "tie" bond was assigned to the contact interface of glass and film. Such a kinematic assumption avoids possible relative translations and rotations for the interested nodes, and it is consequently not able to capture any debonding phenomena, but can offer a rational estimate of vibration response under ideal bonding conditions. For initial numerical considerations, the bond length was kept equal to the size of glass fragments (L_{bond}).

To reproduce the experimental setup in Fig. 2 (linear supports), equivalent nodal restraints were distributed at the end of glass fragments, with $L_{bending} = 95$ mm. Linear modal analyses were carried out to estimate the fundamental frequency and modal shape of fractured, simply supported glass-film samples.

4. Results and discussion

4.1. Experimental records and post-processing

From the present experimental analysis, a set of records and time histories was collected for a total of over 950 impact configurations, grouped by the three series of samples. Fig. 7 (a) an (b) show a typical example of experimental records from the single MEMS sensor in use. It is possible to see multiple impacts (in the form of acceleration or rotation peaks) that were imposed at the mid-pan section for all the samples. Major elaborations and signal processing analyses for the experimental records were carried out with the support of a Matlab® toolbox [40], to express the fundamental vibration frequency of glass-film samples as a function of input / ambient parameters. The analysis of experimental results was further extended by means of FE numerical assessment and comparisons.

4.2. Room temperature performance under repeated impacts

The attention was first focused on the S1-TR set of samples, characterized by vibrations at room temperature and lack of preliminary cooling stage. Typical frequency results can be seen in Fig. 8, where the

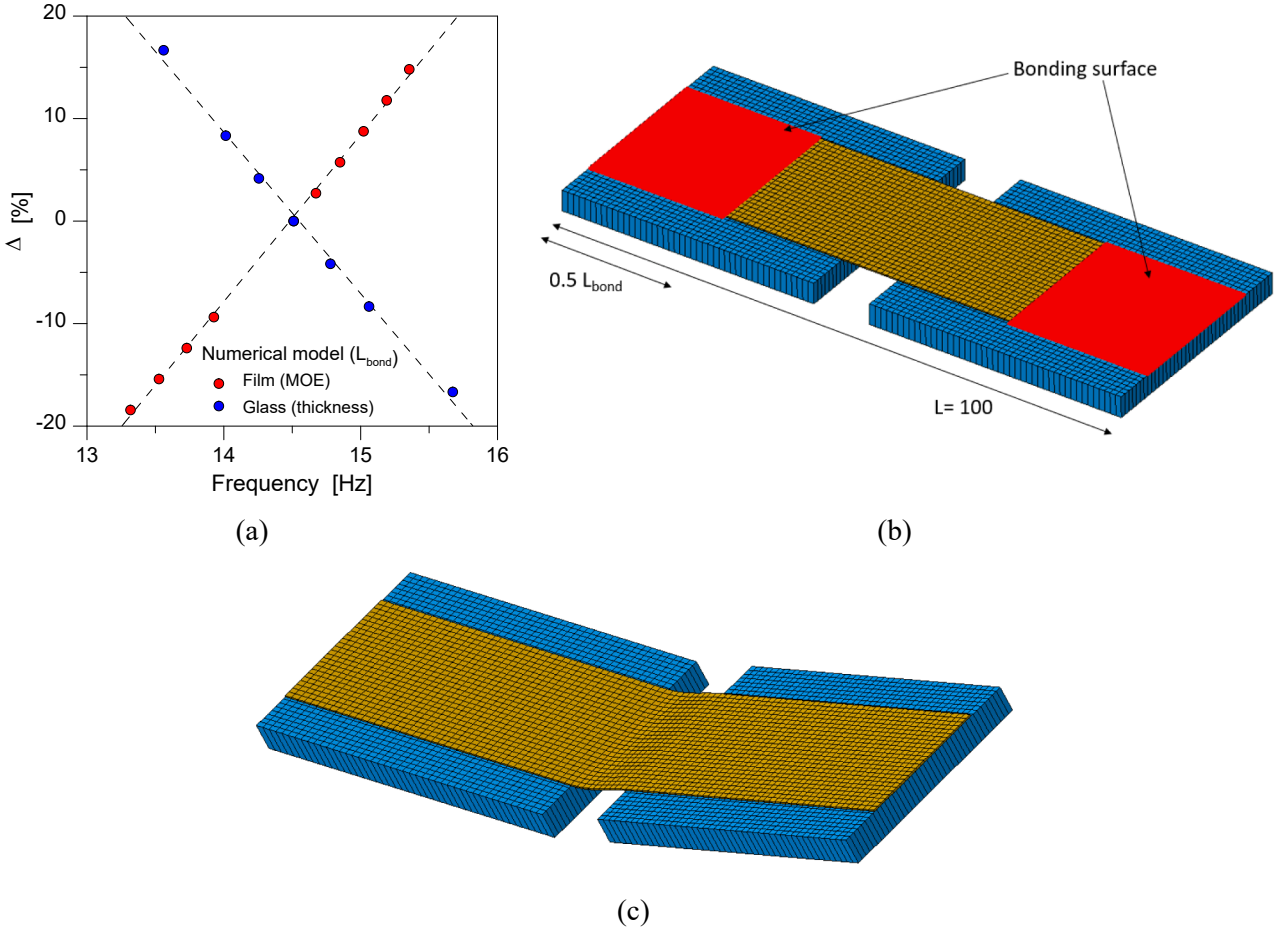

Fig. 9. Parametric numerical analysis: (a) variation of post-fracture vibration frequency with modification of film or glass properties and (b) schematic representation of partial debonding, with (c) corresponding modal shape (ABAQUS). Dimensions in mm.

dynamically identified vibration frequency of glass-film samples is proposed as a function of the acceleration peak for the individual testing conditions, or repetitions respectively. A total of 335 testing scenarios was taken into account. It can be seen that the experimental frequencies were found comprised in a maximum of 14.4 Hz and a minimum of 6.45 Hz, which would correspond, based on the analytical model in Eq. (3), to a single crack extension in the range of $a/t \approx 0.996 \div 0.9982$.

From the set of experimental records is it possible to note, on one side, that the frequency estimates in Fig. 8 (a), as also expected, suggest a certain sensitivity of vibration parameters to possible local effects / variations, such as the stiffness of film, the bond length and / or possible localized delamination (i.e., in the region of fracture, where maximum deflections were imposed to samples), the partial / local contribution of cracked fragments (if any). At the same time, from Fig. 8 (b), it is clear that repeated impacts and vibrations – even in small-scale regime – can strongly affect the residual load-bearing capacity of bonds, and thus of glass-film composite systems. On the other side, a major reduction of fundamental vibration frequency (and thus effective bond for the safety film and equivalent stiffness for the glass-film composite section) can be noted in Fig. 8 (b) especially after the 4th and 5th cycles of imposed impacts. In any case, the two major glass fragments were kept in position in the experimental setup, until the 7th cycle of repeated impacts.

From the same figure, it is worth to note the general trend of frequency values, especially with respect to FE numerical predictions from linear modal analysis. A logarithmic fitting curve is proposed with the 95% confidence interval for the experimental data. Most importantly, in terms of numerical estimates, the blue plot is representative of the glass-film numerical assembly with ideally rigid bond for the contact surfaces as in Fig. 6 (b). At the same time, the numerical analysis is also presented for the same FE model geometry but with a 50 % reduction of bonding surface.

A parametric numerical analysis was in fact carried out to address the sensitivity of numerical frequencies to basic input parameters for the tested glass-film samples. The attention was focused on film stiffness (modulus of elasticity), glass thickness (and thus mass) or even bond length (L_{bond}).

All the calculations were carried out and compared towards the reference "M0" numerical model described in Fig. 6. More precisely, the modulus of elasticity for the safety film was modified in a ± 20 % range, compared to M0. Similarly, the thickness (and thus mass) of glass fragments was changed in a ± 20 % range, compared to M0. Typical results can be seen in Fig. 9 (a) in terms of fundamental frequency modification of the glass-film assembly. Finally, the bond length was also numerically modified, and progressively reduced to account for possible delamination phenomena in the mid-span region of glass,

Table 2
Effect of bond length on the post-fracture fundamental vibration frequency of glass-film samples (selected configurations, ABAQUS).

Model	$m \times L_{bond}$		$f_{1,cr}$ [Hz]	Δf [%]	a/t (Eq. (3))
	Left fragment	Right fragment			
M0	1	1	14.51	–	0.9959
MB-1	1	0.5	8.18	−43.6	0.9977
MB-2	0.5	0.5	6.41	−55.8	0.9982

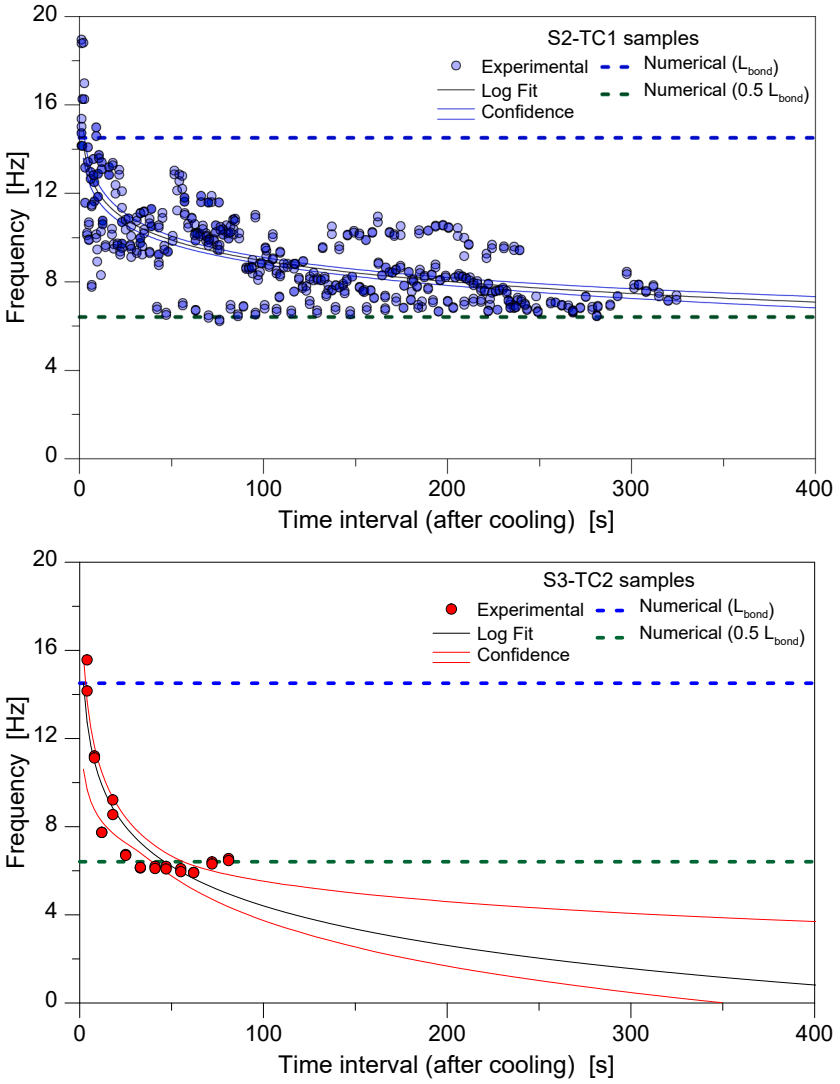

Fig. 10. Experimental results for (a) S2-TRC1 and (b) S3-TC2 samples and comparison with FE numerical estimates (ABAQUS).

where major rotations are expected under repeated bending deformations (Fig. 9 (b)). To this aim, the bond size was reduced down to 50 % the original M0 system, accounting for both symmetrical or unsymmetrical debonding configurations. The typical modal shape can be seen in Fig. 9 (c).

From Fig. 9 and Table 2 is thus possible to note that the most influencing parameter is found in debonding at the mid-span region of samples, while input material and thickness modifications were typically associated to limited modification in fundamental vibration frequency. Most importantly, Table 2 reports also the corresponding a/t ratio, which was analytically calculated from Eq. (3) to fit the numerical cracked frequency. Given that $a/t = 1$ in the corresponding FE assemblies, it is possible to extrapolate from the listed analytical values the safety film contribution, in terms of equivalent stiffness and mechanical continuity to cracked simply supported samples.

4.3. Cooling and temperature gradients effects

For samples in series S2-TC1 and S3-TC2, the attention of experimental results analysis was focused both on the effect of repeated impacts and on the imposed thermal gradients. Due to preliminary cooling stage and a room temperature of 30 °C at the time of impact tests, the reference gradient was in fact quantified in a maximum of $\Delta T = +25$ °C for S2-TC1 samples (from + 5 °C) and $\Delta T = +50$ °C for S3-TC2 samples (from −20 °C). Most importantly, the dynamic experiments were carried out by taking into account a time interval Δt after cooling, and intermediate thermal gradient effects were thus addressed.

Fig. 10 shows the typical experimental results, in terms of post-fracture vibration frequency as a function of time after cooling. Samples are grouped by S2-TC1 and S3-TC2 series respectively, with evidence of the corresponding logarithmic fitting curve (with 95 % confidence level) and FE numerical estimates previously discussed.

It is worth to note, especially for the dynamic experiments carried out immediately after cooling, that the calculated post-fracture vibration frequency is higher than FE numerical estimates and also higher than previous experimental observations for S1-TR samples.

At time 0, the experimental peaks of Fig. 10 can be quantified, based on the analytical model in Eq. (3), in a single crack extension in the order of $a/t \approx 0.996$ and 0.9945 for S2-TC1 and S3-TC2 samples respectively.

Such a minimum stiffening effect could be justified by minor effects of glass fragments interlocking (if any), but also by a positive contribution of low temperatures on the glass-to-film bonding and on the stiffness itself of safety film.

As far as the time interval increases in Fig. 10, both for S2-TC1 and S3-TC2 samples it is in fact possible to see a progressive decrease of calculated vibration frequency, which suggests a decrease in the bending stiffness of the glass-film composite section for each sample. To note that the experimental dots tend to a lower limit frequency value

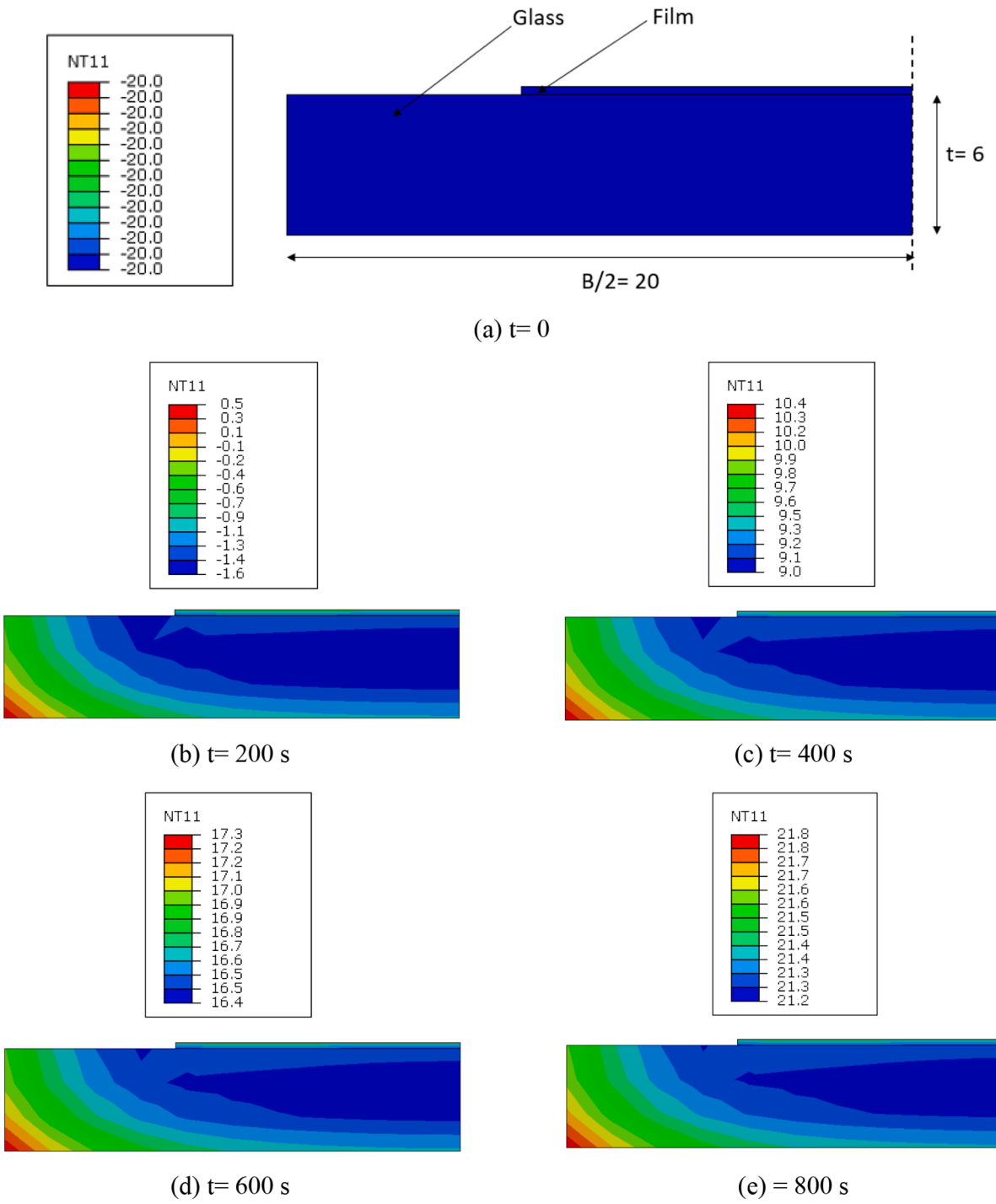

Fig. 11. Temperature evolution in the glass-film sample after cooling (selected contour plots, ABAQUS). Dimensions in mm and temperatures in degrees Celsius.

which again – as it was for the S1-TR samples – is well fitted by FE numerical models with debonding / delamination in the mid-span region of glass. For the S3-TC2 samples, most importantly, the frequency decrease is even more pronounced and premature rather than S2-TC1 samples. Assuming a logarithmic fitting for both the series of samples, in the form:

$$f_{1,cr} = A\ln(\Delta t) + B \tag{6}$$

it is in fact found from Fig. 10 that $A = -1.347$ for series S2-TC1 and $A = -2.590$ for series S3-TC2 respectively. To note that Eq. (6), applied to S1-TR series of samples without thermal gradients, would result in $A = -1.202$, and thus confirm the progressive frequency decrease.

4.4. Numerical analysis of temperature gradients

To further support the interpretation of results, a FE numerical "heat transfer" simulation was also carried out to focus more in detail on temperature evolutions in the typical glass-film sample. To this aim, a primary attention was given to the experimental evidences for S2-TC1 and S3-TC2 subjected to preliminary cooling before dynamic tests at room temperature.

The nominal sample, more precisely, was described in the form of solid brick heat transfer elements from ABAQUS library and exposed to

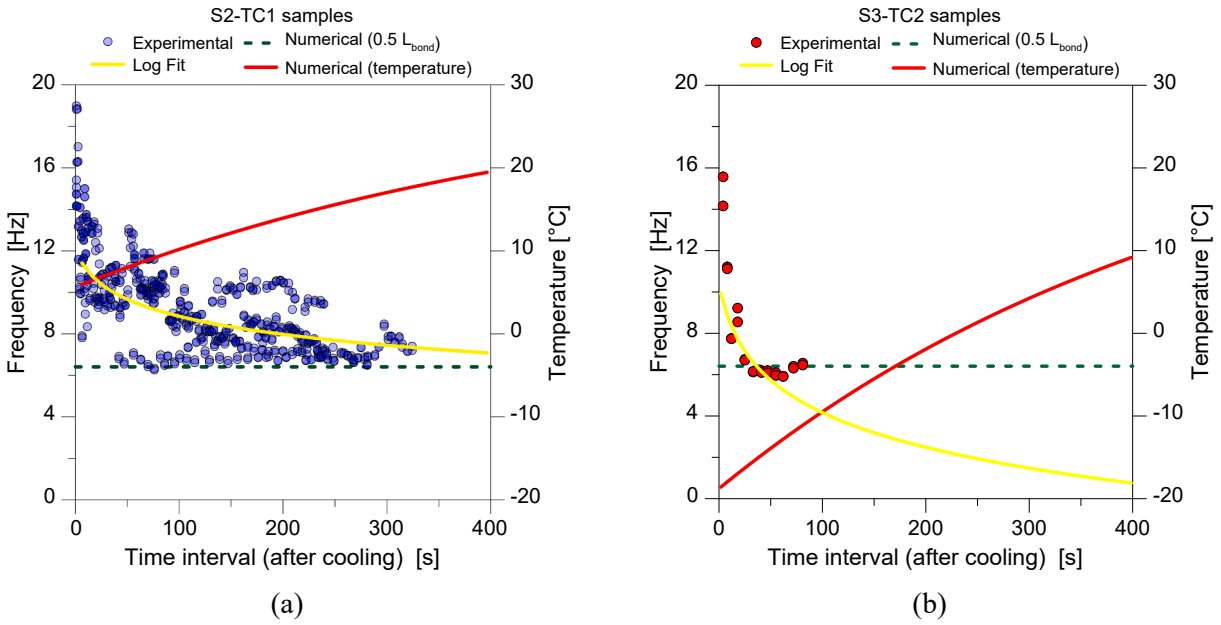

Fig. 12. Post-fracture frequency variation for glass-film samples as a function of time interval after cooling and corresponding temperature, as obtained from experiments and numerical analysis (ABAQUS): (a) S2-TC1 and (b) S3-TC2 samples.

uniform initial temperature of 5 °C or −20 °C respectively, as experimentally done for S2-TC1 and S3-TC2 samples. Accordingly, the room temperature was numerically set in 30 °C as for the experimental setup. The thermal analysis was carried out by monitoring the temperature in time interval after initial cooling, and the progressive temperature increase towards room conditions.

Selected contour plots (half transversal section) are presented in Fig. 11 for S3-TC2 samples. Additional comparative data are reported in Fig. 12.

Especially from Fig. 11, it is worth to note that the uniform temperature of 30 °C in glass and film components was numerically achieved in around ≈ 2600 s after initial cooling (time 0). After a time interval of ≈ 400 s after initial cooling, it is possible to see in Fig. 11 that the average temperature in glass thickness an width is in the order of ≈ 9.5 °C for most of glass section, with temperature peaks (10.4 °C) in the lateral portions of glass only. For the intermediate time interval (i.e., 0 ÷ 400 s), it can be noted in Fig. 11 a rapid temperature increase which can be responsible of major experimental evidences as in Fig. 10, and also suggest further experimental investigations in terms of material and bond characterization under low temperatures. The same numerical outcomes can be also further elaborated in combination with experimental observations.

Fig. 12, more precisely, shows the previously discussed experimental frequency results as a function of the numerically monitored temperature in time, and in particular the measured temperature at the glass-to-film interface after cooling. The logarithmic fitting trend for experimental frequencies is also reported, based on Eq. (6).

It is possible to note that the higher is the measured thermal gradient ΔT at the glass-to-film interface, and the higher is the frequency decrease in the explored time interval. After the first ≈ 100 s after cooling, for example, the S2-TC1 samples are subjected to a thermal gradient $\Delta T = 5$ °C, with a glass-to-film interface temperature in the order of + 10 °C. The corresponding average experimental frequency, based on the logarithmic fitting of Eq. (6), is measured in the order of $f_{1,cr} \approx 9$ Hz, which also corresponds to a crack depth $a/t \approx 0.9975$ from Eq. (3). To note that the experimental post-cracked frequency $f_{1,cr}$ spans in the range ≈ 6.5 ÷ 11.7 Hz, thus corresponding to $a/t \approx 0.9968 \div 0.9982$ based on Eq. (3).

For the S2-TC2 samples, the first 100 s of time interval after cooling are associated to $\Delta T = 11$ °C thermal gradient, with a glass-to-film interface temperature which is numerically estimated in the order of −10 °C, and a corresponding average vibration frequency which is measured in $f_{1,cr} \approx 4.5$ Hz from logarithmic fitting of Eq. (6), that is a crack depth $a/t \approx 0.9987$ from Eq. (3). From experimental data, it is observed that $f_{1,cr} \approx 6$ Hz and $a/t \approx 0.9983$ after 100 s. While the limited number of experimental data for S3-TC2 samples does not support more detailed considerations on thermal gradient effects, the present comparative results suggest in any case that they have – similarly to repeated impact configurations – major effects on bonding efficiency for glass-film samples, and thus on the actual out-of-plane bending stiffness for the examined composite specimens under repeated vibrations.

In this sense, it is thus necessary to further explore the composite behaviour under unfavourable operational conditions, to maximize the structural efficiency and safety of possible retrofit interventions.

5. Conclusions

In engineering applications, structural glass solutions in combination with polymers can suffer for mechanical degradation as a consequence of unfavourable operational conditions, ambient, temperature, etc., with major effects on load-bearing performances and safety levels.

In this paper, the attention was focused on annealed, monolithic glass samples bonded by commercial safety films of typical use for retrofit, which are based on Polyethylene terephthalate (PET)-layers and pressure sensitive adhesives (PSAs). An experimental investigation was carried out to address and quantify the effects of post-fracture repeated impacts and thermal gradients on glass-film composites. Based on a small-scale laboratory setup of cracked composite beams on simply supports (single major crack), a total of 950 configurations was investigated in terms of impact conditions and preliminary thermal treatment.

The interpretation of dynamic experimental results was carried out in terms of post-fracture fundamental vibration frequency (based on classical identification techniques), with the support of simplified analytical estimates and Finite Element (FE) numerical simulations.

Overall, the mechanical characterization of glass-film samples under low-amplitude vibrations was successfully used to quantify their residual load-bearing capacity under unfavourable conditions, and thus to

address the robustness of similar retrofit interventions. Most importantly, it was shown that even under repeated impact cycles, the selected bonding films can still offer a certain mechanical continuity to glass fragments, which is of primary importance for post-fracture redundancy. On the other side, a marked and progressive decrease in the corresponding vibration frequency, and thus in the corresponding mechanical coupling of glass and safety film, was also measured from experiments. In terms of analytical calculations, the mechanical bonding and structural continuity offered by safety films to cracked glass fragments was measured in about an equivalent $a/t \approx 0.99$ ratio of crack depth a, compared to the glass thickness t. On the other side, it was also shown that short-term thermal gradients may be responsible of major debonding in the region of cracks, and thus reduce further the composite action of the glass-film system under vibrations.

Data availability

Data will be shared upon request.

CRediT authorship contribution statement

Chiara Bedon: Conceptualization, Methodology, Data curation, Investigation, Validation, Software, Writing – original draft, Writing – review & editing, Project administration, Supervision. **Filipe A. Santos:** Data curation, Investigation, Writing – original draft, Writing – review & editing.

Declaration of Competing Interest

The authors declare that they have no known competing financial interests or personal relationships that could have appeared to influence the work reported in this paper.

Data availability

Data will be made available on request.

Acknowledgements

This research study was financially supported by University of Trieste (“Microgrants 2020” grant, D13_microgrants_BEDON).

Seretti Srl (San Giorgio di Nogaro, Italy) is acknowledged for offering the monolithic glass samples.

References

[1] Bedon C, Santarsiero M. Transparency in Structural Glass Systems Via Mechanical, Adhesive, and Laminated Connections - Existing Research and Developments. Adv Eng Mater 2018;20(5):1700815.
[2] Tserpes K, Barroso-Caro A, Carraro PA, Beber VC, Floros I, Gamon W, et al. A review on failure theories and simulation models for adhesive joints. J Adhes 2022;98(12):1855–915.
[3] Van Lancker B, Dispersyn J, De Corte W, Belis J. Durability of adhesive glass-metal connections for structural applications. Eng Struct 2016;126:237–51.
[4] Machalická K, Eliášová M. Adhesive joints in glass structures: effects of various materials in the connection, thickness of the adhesive layer, and ageing. Int J Adhes Adhes 2017;72:10–22.
[5] Denonville J, Puller K, Haase W, Sobek W. Long-term Behaviour of Metal Inserts Partially Embedded in Laminated Glass. Glasbau 2013;2013:117–27.
[6] Bedon C, Santarsiero M. Laminated glass beams with thick embedded connections-Numerical analysis of full-scale specimens during cracking regime. Compos Struct 2018;195:308–24.
[7] Volakos E, Davis C, Teich M, Lenk P, Overend M. Structural performance of a novel liquid-laminated embedded connection for glass. Glass Struct Eng 2021;6:487–510. https://doi.org/10.1007/s40940-021-00162-w.
[8] Mattei S, Cozzarini L, Bedon C. Experimental and Numerical Peeling Investigation on Aged Multi-Layer Anti-Shatter Safety Films (ASFs) for Structural Glass Retrofit. Symmetry 2022;14:162. https://doi.org/10.3390/sym14010162.
[9] Bedon C, Mattei S. Multistep Experimental Calibration of Mechanical Parameters for Modelling Multilayer Antishatter Safety Films in Structural Glass Protection. Mathematical Problems in Engineering, vol. 2021, Article ID 6714418, 14 pages; 2021. https://doi.org/10.1155/2021/6714418.
[10] Mattei S, Cozzarini L, Bedon C. Pre- and Post-Failure Experimental Bending Analysis of Glass Elements Coated by Aged Anti-Shatter Safety Films. Proceedings of Challenging Glass 8, vol. 8; 2022, doi: https://doi.org/10.47982/cgc.8.401.
[11] Volakos E, Davis C, Teich M, Lenk P, Overend M. Temperature effects on the behaviour of liquid-laminated embedded glass connections. Eng Struct 2023;274:115164. https://doi.org/10.1016/j.engstruct.2022.115164.
[12] Serafinavičius T, Lebet JP, Louter C, Lenkimas C, Kuranovas A. Long-term laminated glass four point bending test with PVB, EVA and SG interlayers at different temperatures. Proc Eng 2013;57:996–1004.
[13] Hána T, Vokáč M, Eliášová M, V. Machalická K. Experimental investigation of temperature and loading rate effects on the initial shear stiffness of polymeric interlayers. Eng Struct 2020;223:110728.
[14] Pelayo F, Lamela-Rey MJ, Muniz-Calvente M, López-Aenlle M, Álvarez-Vázquez A, Fernández-Canteli A. Study of the time-temperature-dependent behaviour of PVB: application to laminated glass elements. Thin-Walled Struct 2017;119:324–31.
[15] Katsivalis I, Thomsen OT, Feih S, Achintha M. Effect of elevated temperatures and humidity on glass/steel adhesive joints. Int J Adhesion Adhes 2020;102:102691.
[16] Stazi F, Giampaoli M, Tittarelli F, Di Perna C, Munafò P. Durability of different glass coatings in humid and saline environments, ageing impact on heat-light transmission and thermal comfort. Build Environ 2016;105:210–24.
[17] Mariggiò G, Dalle Vacche S, Bongiovanni R, Louter C, Corrado M. A durable coating to prevent stress corrosion effects on the surface strength of annealed glass. Glass Structures and Engineering 2021;6(4):449–62.
[18] Van Dam S, Pelfrene J, De Pauw S, Van Paepegem W. Experimental study on the dynamic behaviour of glass fitted with safety window film with a small-scale drop weight set-up. Int J Impact Eng 2014;73:101–11.
[19] Figuli L, Papan D, Papanova S, Bedon C. Experimental mechanical analysis of traditional in-service glass windows subjected to dynamic tests and hard body impact. Smart Struct Syst 2021;27:365–78.
[20] Jefferson Andrew J, Arumugam V, Saravanakumar K, Dhakal HN, Santulli C. Compression after impact strength of repaired GFRP composite laminates under repeated impact loading. Compos Struct 2015;133:911–20.
[21] Ozdemir O, Oztoprak N, Kandas H. Single and repeated impact behaviors of bio-sandwich structures consisting of thermoplastic face sheets and different balsa core thicknesses. Compos B Eng 2018;149:49–57.
[22] Acar Yavuz G, Gören Kıral B, Hızarcı B, Kıral Z. Low-velocity single and repeated impact behavior of 3D printed honeycomb cellular panels. Materials Testing 2022;64(10):1420–36.
[23] Bedon C. Issues on the Vibration Analysis of In-Service Laminated Glass Structures: Analytical, Experimental and Numerical Investigations on Delaminated Beams. Appl Sci 2019;9(18):3928. https://doi.org/10.3390/app9183928.
[24] Zhang Z, Shankar K, Morozov EV. Tahtali, M. Vibration-based delamination detection in composite beams through frequency changes. J Vib Control 2016;22:496–512.
[25] Krawczuk M, Ostachowicz W, Zak A. Analysis of natural frequencies of delaminated composite beams based on finite element method. Struct Eng Mech 1996;4(3):243–55.
[26] Vedrtnam A. Experimental and simulation studies on delamination strength of laminated glass composites having polyvinyl butyral and ethyl vinyl acetate interlayers of different critical thicknesses. Def Technol 2018;14(4):313–7.
[27] Bedon C. Diagnostic analysis and dynamic identification of a glass suspension footbridge via on-site vibration experiments and FE numerical modelling. Compos Struct 2019;216:366–78.
[28] Bedon C, Fasan M, Amadio C. Vibration analysis and dynamic characterization of structural glass elements with different restraints based on Operational Modal Analysis. Buildings 2019;9(1):13.
[29] Clough RW, Penzien J. Dynamics of Structures; McGraw-Hill: New York, NY, USA, ISBN 0-07-011394-7; 1993.
[30] Bedon C, Santi MV, Fasan M. Considerations on efficient procedural steps for seismic capacity assessment and diagnostics of historic structural glass systems. Soil Dyn Earthq Eng 2022;163:107562.
[31] Fernandez-Saez J, Rubio L, Navarro C. Approximate calculation of the fundamental frequency for bending vibrations of cracked beams. J Sound Vib 1999;225(2):345–52.
[32] Andreozzi L, Bati SB, Fagone M, Ranocchiai G, Zulli F. Dynamic torsion tests to characterize the thermo-viscoelastic properties of polymeric interlayers for laminated glass. Constr Build Mater 2014;65:1–13.
[33] Vokáč M, Hána T, Machalická K, Eliášová M. Viscoelastic Properties of PVB Interlayer for Laminated Glass Structures Used in Building Reconstructions. Key Eng Mater 2019;808:115–22.
[34] Salgado-Pizarro R, Castro JR, Cabeza LF. Viscoelastic characterization of seven laminated glass interlayer materials from static tests. Constr Build Mater 2021;279:122503.
[35] López-Aenlle M, Noriega A, Pelayo F. Mechanical characterization of polyvinil butyral from static and modal tests on laminated glass beams. Composites B 2019;169:9–18.
[36] Simulia, Abaqus computer software, v. 6.14; 2022.
[37] Galuppi L, Royer-Carfagni G. Effective thickness of laminated glass beams: New expression via a variational approach. Eng Struct 2012;38:53–67.
[38] Galuppi L, Royer-Carfagni G. The design of laminated glass under time-dependent loading Int. J Mech Sci 2013;68:67–75.
[39] EN 572–2:2004. Glass in buildings – Basic soda lime silicate glass products. CEN, Brussels, Belgium.
[40] MATLAB (R2018a); Version 9.4 Natick; The MathWorks Inc.: Natick, MA, USA.